Heliyon 8 (2022) e10042

Contents lists available at ScienceDirect

Heliyon

journal homepage: www.cell.com/heliyon

Research article

Apatitic calcium phosphate/montmorillonite nano-biocomposite: in-situ synthesis, characterization and dissolution properties

M. Jamil [a,b,*], A. Elouahli [a], F. Abida [a], J. Assaoui [a], E. Gourri [a], Z. Hatim [a]

[a] Team of Energy, Materials and Environment, Department of Chemistry, Faculty of Sciences, University of Chouaib Doukkali, El Jadida, Morocco
[b] Team of Mineral Solid Chemistry, Laboratory of Applied Chemistry and Environment, Department of Chemistry, Faculty of Sciences, Mohammed First University, Oujda, Morocco

ARTICLE INFO

Keywords:
Montmorillonite
Apatitic calcium phosphate
In-situ precipitation
Silicate biocomposites
Multiphasic biocomposite
Dissolution

ABSTRACT

Recently, calcium phosphate/montmorillonite composites have received attention as a synthetic bone substitutes. In this study, apatitic calcium phosphate/Montmorillonite nano-biocomposites were in-situ synthesized at 22 °C by reaction between calcium hydroxide and orthophosphoric acid in the presence of different contents of montmorillonite (MNa). Fourier Transform Infrared Spectroscopy (FTIR), X-ray Diffraction (XRD), Transmission Electron Microscopy (TEM) and Brunauer–Emmett–Teller (BET) surface areas were used to characterize the prepared powders. The XRD results show that the composites prepared with 2 and 5 wt% MNa and sintered at 900 °C, show the formation of hydroxyapatite (HAP) structure, whereas that prepared with 10 wt% MNa leads to the formation of β-tricalcium phosphate (β-TCP) structure. The HAP structure decomposes at 1000 °C and leads to the formation of biocomposite containing HAP, β and α-TCP. However, β-TCP composites show thermal stability. FTIR and structural refinement results show the incorporation of clay ions into the apatitic structure causing changes in the crystal structure of the formed calcium phosphate phases. The changes in the composition and structure lead to an increase in the dissolution rate of HAP and a decrease in that of β-TCP.

1. Introduction

Hydroxyapatite ($Ca_{10}(PO_4)_6(OH)_2$: HAP) is widely used as a bone substitute due to its structure similar to the mineral part of the bone tissue [1]. However, HAP has several disadvantages, such as slow biodegradation during the repair of bone defects [2]. Tricalcium phosphate β ($Ca_3(PO_4)_2$: β-TCP) has also received considerable attention as a bone substitute for its excellent biodegradation and good biocompatibility [3, 4]. However, although β-TCP is biocompatible, it shows a weak bioactivity [5]. Recently, it was reported that the chemical and biological properties of HAP and β-TCP may be improved by their association with metals [6], organic compounds [7] or by the substitution of foreign ions in their crystal structure as Na^+ [8, 9], Mg^{2+} [10], Sr^{2+}/F^- [11], SiO_4^{4-} [12] and Al^{3+} [13]. Biological apatite is non-stoichiometric due to the presence of a different oligo-elements as Zn^{2+}, Mg^{2+}, Na^+, CO_3^{2-} [14, 15], which play an important role in biological processes related to bone and connective tissue development [16, 17].

Montmorillonite belongs to Smectites group which the individual layers are composed of a central octahedral of aluminum hydroxide sheet fused in between two silica tetrahedral sheets. The layers of montmorillonite-clay carry a negative charge due to isomorphous substitution in tetrahedral (Al^{3+} for Si^{4+}) and octahedral (Mg^{2+} for Al^{3+}) layers, which is compensated by exchangeable alkaline or earth alkaline cations as K^+, Na^+, Ca^{2+} occupying interlayer space [18]. Therefore, montmorillonite has a high swelling capacity, high cation exchange capacity and large surface area [19]. These properties make montmorillonite-clay useful in pharmaceutical applications as excipients, as drug delivery system [20, 21], or associated with polymers, metals or ceramics to prepare biocomposites [22, 23, 24, 25, 26]. Indeed, in recent years the development of composite based on calcium phosphate/montmorillonite has attracted great attention for biomedical applications. Several studies have reported the preparation of hydroxyapatite/montmorillonite composites either by precipitation in an aqueous medium [23, 27, 28, 29] or by sintering method [24, 25]. Various studies have reported an improvement of the mechanical and biological properties of the calcium phosphate/-montmorillonite composite [23, 27, 28, 29, 30, 31].

In recent study the authors reported the preparation of β-tricalcium phosphate/montmorillonite composite by sintering powder of apatitic tricalcium phosphate in the presence of Na-montmorillonite (MNa) [26]. We showed that the thermal interaction between calcium-apatite

* Corresponding author.
E-mail address: mo.jamil@yahoo.fr (M. Jamil).

https://doi.org/10.1016/j.heliyon.2022.e10042
Received 8 August 2021; Received in revised form 19 March 2022; Accepted 18 July 2022

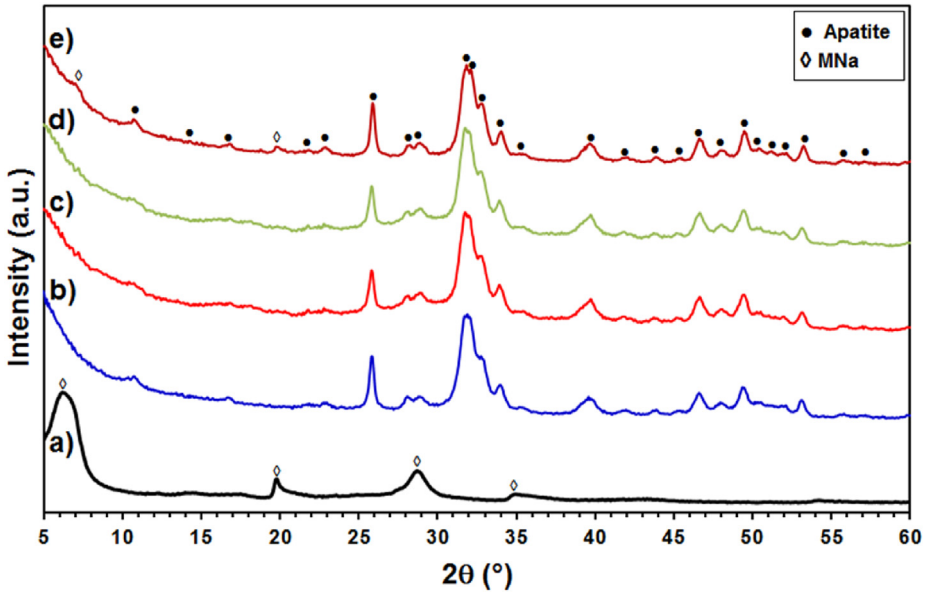

Figure 1. XRD patterns of as-synthesized powders a) AP-0MNa, b) AP-2MNa, c) AP-5MNa and d) AP-10MNa.

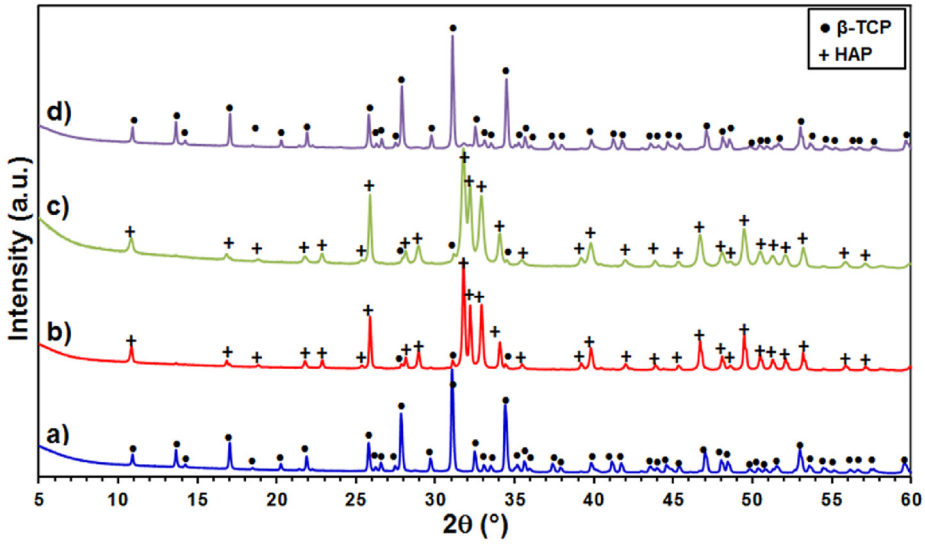

Figure 2. XRD patterns of sintered samples at 900 °C: a) AP-0MNa, b) AP-2MNa, c) AP-5MNa and AP-10MNa.

and MNa leads to the formation and stabilization of β-TCP substituted by clay ions. We have also reported, in other works, that during the sintering, interaction of MNa and apatite powders with two desired Ca/P molar ratios (1.660 and 1.623) led to the decomposition of apatite and formation of composite ceramics comprising HAP, β and α-TCP [25].

In the literature, it is increasingly known that the combination of calcium phosphate and montmorillonite leads to better biological and mechanical properties of the resulting composites. The main advantage of these biomaterials can be their ability to release: Ca, P and clay ions as silicon, sodium and magnesium which stimulate bone growth and ensure good biological compatibility. Therefore, the development of new materials combining hydroxyapatite, tricalcium phosphate and montmorillonite may be of great interest for various medical applications and it becomes necessary to understand the effect of the clay phase on their composition and structure.

The present study concerns the development of new class of biocomposites combining apatitic calcium phosphate and montmorillonite. We have prepared, by *in-situ* precipitation in an aqueous medium, apatitic calcium phosphate/montmorillonite nano-biocomposites. We have studied the effect of the clay phase on the structure, composition, thermal stability and dissolution of the resulting composites.

2. Materials and methods

2.1. Materials

The starting reagents were Na-montmorillonite, $CaCO_3$ and H_3PO_4. The sodium montmorillonite (MNa) (Cloisite-Na^+) was obtained from Southern Clay Products, Inc. The cation exchange capacity (CEC) is 92.6 meq/100 g of montmorillonite. The composition of MNa as follows (wt %): Na_2O 7.223, MgO 4.133, Al_2O_3 19.986, SiO_2 56.851, P_2O_5 0.022, K_2O 0.442, CaO 0.698, MnO 0.053, TiO 0.368, and Fe_2O_3 7.936.

$CaCO_3$ (Skora, Analytical grade) and H_3PO_4 (Merck, Analytical grade) were selected as starting chemical precursors for calcium and phosphorus elements.

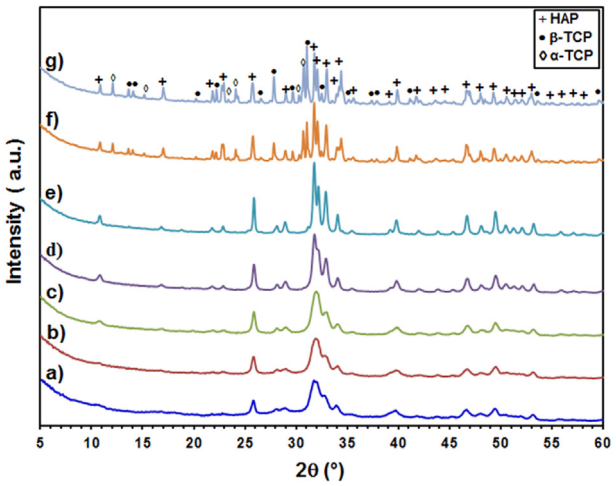

Figure 3. XRD patterns of a) dried AP-5MNa at 105 °C and heat treated at b) 200 °C, c) 500 °C, d) 700 °C, e) 900 °C, f) 1000 °C and g) 1100 °C.

2.2. Powder synthesis

The neutralization method, previously reported by Elouahli A. et al [32], was used for the synthesis of apatitic calcium phosphate/MNa (AP-MNa) composite. This method is non-polluting; the reagents are simple without any counter ions. Initially, the calcium oxide powder, prepared by sintering $CaCO_3$, was dispersed in bidistilled water. MNa was added as a fine powder, under stirring, in a suspension of $Ca(OH)_2$ (0.5 mol/L) with concentration of 2, 5 and 10% by weight relative to the weight of apatite. The orthophosphoric acid solution (1 mol/L) was added at 22 °C with an addition rate of 33 ml/min to the MNa-$Ca(OH)_2$ suspension using vigorous stirring (470 rpm). The Ca/P molar ratio of the reagents was 1.50 ± 0.02. The resulting precipitates were filtered, dried at 105 °C overnight and stored at grain size less than 125 μm.

According to the added quantity of MNa (x), the AP-xMNa nanocomposites are named: AP-0MNa, AP-2MNa, AP-5MNa and AP-10MNa.

The prepared AP-5MNa and AP-10MNa composites were heat treated at different temperatures until 1100 °C for 3h under air atmosphere.

2.3. Characterization

Infrared spectra of powders were carried out on a Fourier Transform Spectrometer (SHIMADZU FTIR-8400S) in the spectral range of 400–4000 cm^{-1} with a resolution of 4 cm^{-1} and 20 scans. The powder samples were mixed and ground with KBr (1%) and then pressed in a 13 mm die.

Table 1. Characteristics of prepared samples: AP-2MNa, AP-5MNa and theoretical hydroxyapatite HAP_{THE}.

Samples	a (Å)	c (Å)	V (Å^3)	D_{ind}	D_{300} (nm)	D_{002} (nm)
HAP_{THE}	9.4190	6.8800	529.16	3.07	-	-
AP-2MNa	9.4044	6.8664	525.92	13.34	61.21	92.23
AP-5MNa	9.4080	6.8690	526.52	27.55	28.62	48.01

Phase compositions of the dried and sintered powders were determined by a BRUKER D8 ADVANCE diffractometer using copper K_α radiation ($\lambda = 1.5406$ Å). FullProf program (WinPLOTR 2017) was used to perform the structural characterization for the prepared samples. The distortion of the structure can be estimated from the distortion of the PO_4 tetrahedrons. The tetrahedral distortion index was calculated according to Eq. (1):

$$D_{ind} = \frac{\sum_{i=1}^{6}(OPO_i - OPO_m)^2}{6} \quad (1)$$

where OPO_i represents the six angles between P and the four O atoms of the phosphate tetrahedron and OPO_m is the average angle (around 109.17°).

The Scherrer formula (Eq. (2)) was adopted to calculate the crystallite size of the calcined samples [33, 34]:

$$L = 0.9\lambda/\beta\cos\theta \quad (2)$$

where λ is the wavelength of the used Cu-K_α radiation, β is the full width at the half maximum of the HAP line and θ is the diffraction angle.

The concentrations of calcium, phosphorus and silicone were determined by inductively coupled plasma atomic emission spectrometry (ICP-AES) (ThermoJarrel Ash. Atom Scan 16). Specific surface area was measured by the BET method (Micromeritics ASAP 2010). The microstructure of samples was examined through Electron Microscopy TEM (TalosF200S).

2.4. Dissolution tests

The dissolution tests were conducted in acidic medium at pH 4.8 ± 0.2 related to the in vivo degradation of the phosphocalcic implants [35, 36]. The sintered powders at 900 °C for 3 h were ground and 125

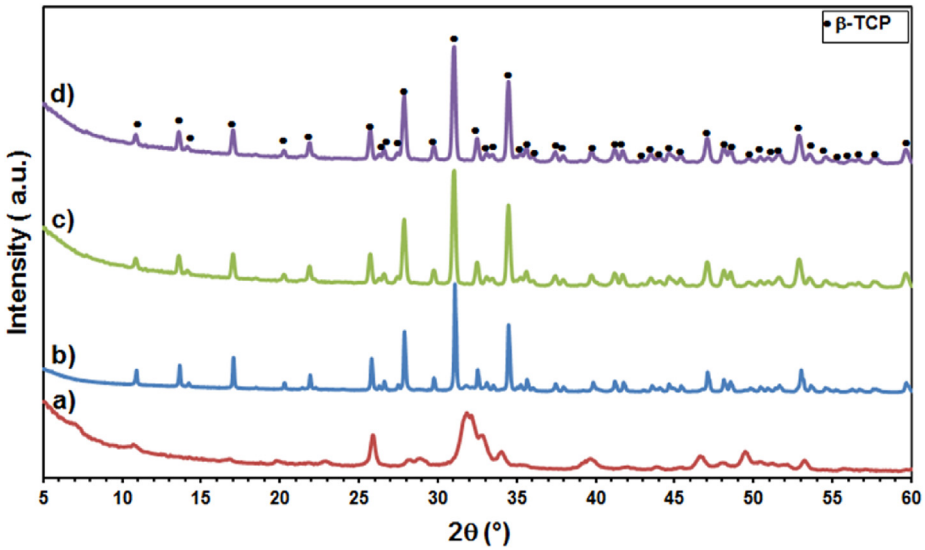

Figure 4. XRD patterns of a) dried AP-10MNa at 105 °C and heat treated at b) 900 °C, c) 1000 °C and d) 1100 °C.

Table 2. Characteristics of prepared samples AP-0MNa and AP-10MNa.

Samples	a (Å)	c (Å)	V (Å^3)	D_{ind}	D_{300} (nm)	D_{214} (nm)
AP-0MNa	10.4128	37.3645	3508.5608	25.26	81.63	87.80
AP-10MNa	10.3884	37.3413	3489.9490	29.09	96.65	94.60

μm-sieved. 200 mg of powder was soaked under agitation in acetate buffer solution (100 ml) with pH = 4.8 ± 0.2 and temperature of 37.0 ± 0.1 °C for various periods. After soaking, the liquid phase was separated and the ionic concentration of the solution was analyzed by ICP-AES.

3. Results and discussion

3.1. Structural analysis and rietveld refinement

The XRD patterns of as-synthesized powders AP-xMNa are presented in Figure 1. Overall, the XRD peaks in the all patterns are wide and reveal the formation of a single phase, with a low crystallinity, characteristics of apatitic structure (ICDD-PDF n° 09–0432). Figure 1(d) indicates the presence of diffraction peaks characteristics of MNa phase visible in the case of AP-10MNa sample.

XRD patterns of the calcined powders at 900 °C are given in Figure 2. The XRD pattern (Figure 2(a)) of the powder AP-0MNa, prepared without MNa, shows a single well-crystalized phase corresponding to β-TCP (ICCD-PDF n° 09–0169). Indeed, the apatitic tricalcium phosphate transforms after calcination to β-TCP phase according to Eq. (3), in relation with the Ca/P molar ratio of reagents (Ca/P equal to 1.50).

$$Ca_9(HPO_4)(PO_4)_5(OH) \rightarrow 3Ca_3(PO_4)_2 + \ H_2O \quad (3)$$

While, XRD patterns (Figure 2b and c) of AP-2MNa and AP-5MNa composites show the formation of crystallized HAP phase (ICCD-PDF n° 09–432). However, the XRD pattern of the AP-10MNa composite shows the formation of β-TCP phase.

The results show that the addition of MNa affected the type of the formed calcium phosphate phases in the composites. This suggests that there is an incorporation of the clay ions into the apatitic structure stabilizing HAP or β-TCP structure, depending to the amount of the added MNa. This incorporation of clay ions takes place particularly during the precipitation of apatitic crystals. This was confirmed by the case of preparation where the clay was added after the addition of orthophosphoric acid (i.e. after precipitation of the apatitic calcium phosphate). In this case, a β-TCP structure which formed independent on the amount of MNa (results not shown).

The incorporation of clay ions into the apatitic structure can have two origins. The first source is the ionic exchange between interlayer cations of montmorillonite and cationic species in the medium because Na-montmorillonite is characterized by a very high cation exchange capacity. The second source is the partial dissolution of MNa in the nucleation medium because the montmorillonite dissolves in a basic medium and that its dissolution rate increases with increasing pH and temperature [37, 38]. In this study, MNa was added to a high alkaline suspension of calcium hydroxide (pH = 12) which promotes a partial dissolution of MNa and therefore the clay ions (e.g. SiO_4^{4-}, Al^{3+}, Mg^{2+} and Na^{+}) can be released into the medium and incorporated into the apatitic structure during its nucleation.

The insertion of clay ions into the apatitic structure can also take place during calcination. Indeed, in recently work, we have prepared β-tricalcium phosphate bioceramics by sintering process at 900 °C of apatitic calcium phosphate powder (molar ratio Ca/P 1.50) in the presence of MNa [26]. We have found that during sintering, interaction apatite-MNa led to the incorporation of clay ions into the apatite structure which stabilized the formed β-TCP. More recently, we have also reported that, during the sintering, an interaction between MNa and apatite powders with two desired Ca/P molar ratios (1.660 and 1.623) have led to the decomposition of the apatite, at relatively low temperature, and formation of composite ceramics comprising HAP, β and α-TCP [25]. So, the obtained results confirm the incorporation of clay ions and decomposition of the apatitic structure during the heat treatment.

In the present study, the incorporation of clay ions into the apatitic structure with atomic ratio Ca/P equal to 1.50 takes places principally during its nucleation. Depended on the amount of MNa, the biocomposites sintered at 900 °C leads to the formation of the HAP or β-TCP structure. For low amounts of MNa, the incorporation of clay ions promotes the formation of HAP structure. However, for high amounts of MNa, the incorporation of clay ions stabilizes a β-TCP structure. The substitution of a sufficient quantity of the Mg clay ion seems to lead to the stability of the TCP phase. Indeed, various studies have reported that Mg ions stabilize the β-TCP phase, even in small quantities [39, 40].

The AP-5MNa and AP-10MNa composites were subjected to heat treatment at different temperatures until 1100 °C in order to analyze their thermal behavior.

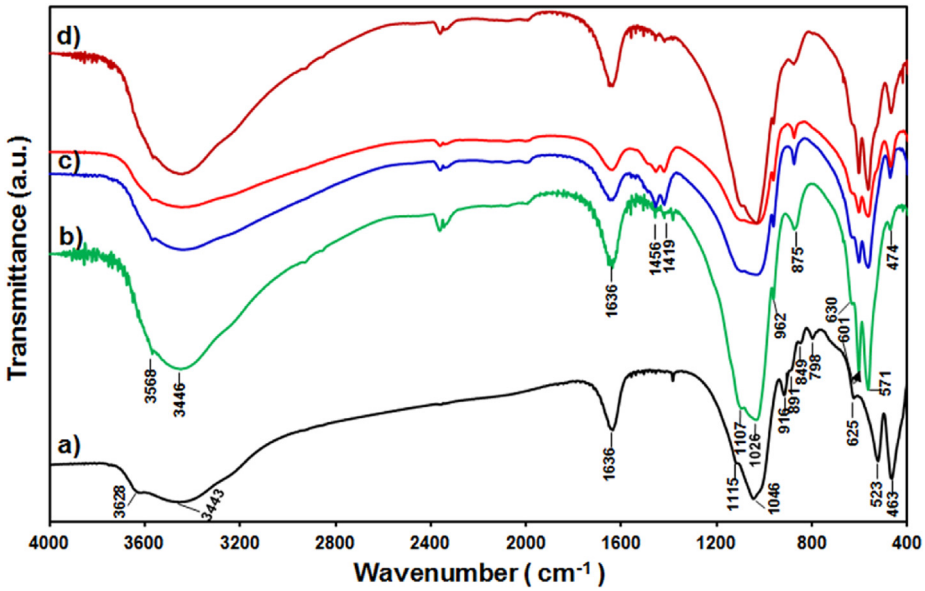

Figure 5. FTIR spectra of the dried powders: a) AP-0MNa, b) AP-2MNa, c) AP-5MNa and d) AP-10MNa.

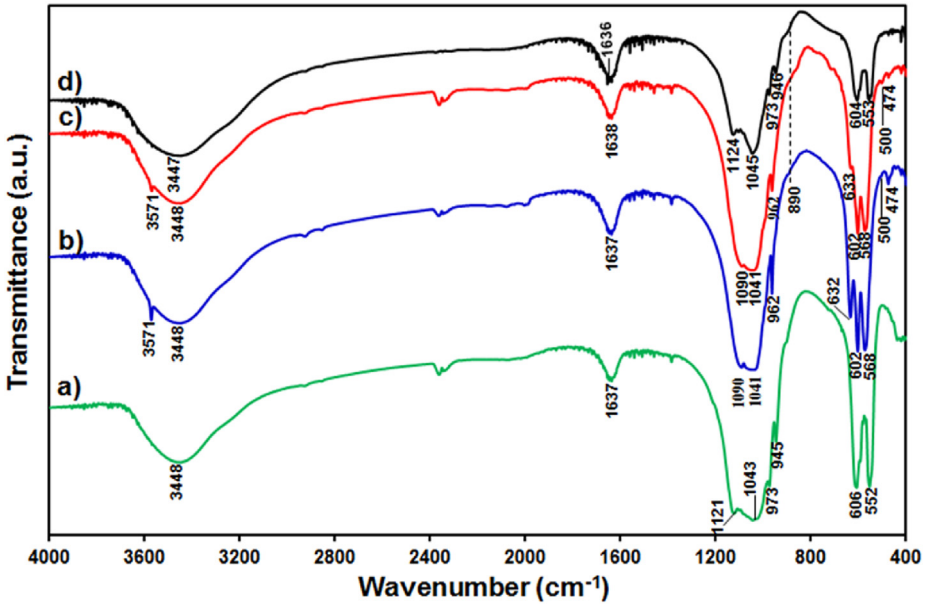

Figure 6. FTIR spectra of the sintered samples at 900 °C: a) AP-0MNa, b) AP-2MNa, c) AP-5MNa and d) AP-10MNa.

Figure 3 shows the XRD patterns of dried and heat treated AP-5MNa at temperature from 200 °C to 1100 °C. The diffraction peaks of the dried powder are wide which reveal a low crystallinity of the as-synthesized apatite. This phase became better crystallized in between 700 °C and 900 °C. Two new phases: β-TCP and α-TCP appear at 1000 °C and their diffraction intensities increase with increasing temperature. These results indicate the decomposition of the HAP structure leading to the formation of α-TCP phase at a relatively low temperature. We specify that the α-TCP is generally stable at higher temperatures (>1125 °C) [41, 42].

However, as shown in Figure 4, the XRD patterns of the sintered AP-10MNa until 1100 °C show a single β-TCP phase and the absence of any other phase. This result reveals that the quantity of Mg involved during the apatite-MNa interaction stabilizes the β-TCP structure in accordance with the previous study [26].

The Rietveld refinement results of the calcined powders AP-xMNa at 900 °C are presented in Tables 1 and 2.

The results (Table 1) show that the crystalline parameters (a and c) and the cell volume of the HAP decreased with the addition of 2 wt% of MNa compared to theoretical values, and then increase slightly with the addition of 5 wt% of MNa. These structural changes cause a distortion of the crystal lattice of the HAP structure. Indeed, the distortion index D_{ind} undergoes an increase with the increase of the MNa content.

The results of Table 2 show that the crystal parameters (a and c) and the cell volume decrease of the β-TCP with the addition of 10 wt% MNa, compared to the pure β-TCP. However the distortion index D_{ind} undergoes an increase with the increase of the MNa content.

The results reveal that MNa affected the thermal stability and the crystalline parameters of the formed calcium phosphate phases which confirm the incorporation of clay ions in to the apatitic structure.

3.2. FTIR analysis

The FTIR spectra of the dried AP-xMNa (x = 0, 2, 5 and 10 wt%) powders are presented in Figure 5. All FTIR spectra show the presence of the vibration bands characteristic of an apatitic structure. The vibration bands attributable to H_2O (around 3446 and 1636 cm^{-1}), HPO_4^{2-} groups (875 cm^{-1}) and hydroxyl ions OH^- (630, 3568 cm^{-1}) are noted. The bands around 1107, 1026, 962, 571, 601 and 474 cm^{-1} attributable to the

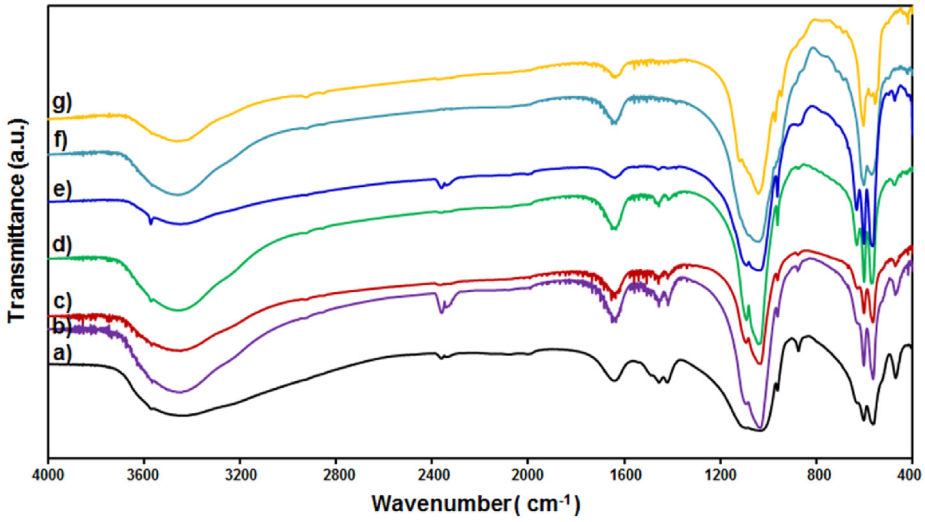

Figure 7. FTIR spectra of the AP-5MNa powder as a function of heat treatment at temperature from 200 °C to1100 °C.

Table 3. Specific surface area values of the synthesized powders.

Sample	AP-0MNa	AP-2MNa	AP-5MNa	AP-10MNa
SSA ($m^2\ g^{-1}$)	80.00	100.15	90.47	52.99

vibrations of PO_4^{3-} groups. We can also observe the presence of bands around 1419 and 1456 cm^{-1} attributed to carbonates CO_3^{2-}.This is due to the incorporation of atmospheric CO_2 in the alkaline $Ca(OH)_2$-MNa medium.

The FTIR spectra of the sintered powders at 900 °C for 3h are presented in Figure 6. The FTIR spectrum (Figure 6(a)) of the sintered reference sample AP-0MNa shows the bands at 552, 606, 945, 973, 1043 and 1121 cm^{-1} attributed to the vibration of PO_4 groups in the β-TCP structure. FTIR spectra (Figure 6b and c) of the sample AP-2MNa and AP-5MNa show the bands of PO_4 groups (1090, 1041, 962, 602, 568 and 474 cm^{-1}) and OH group (3571 and 632 cm^{-1}) characteristic in hydroxyapatite structure. In addition, we can observe two new bands located at 890 and 500 cm^{-1} attributed to the vibrations of the Si–O bond in the SiO_4 group [43]. As shown in Figure 6b and c, there is loss intensity in OH^- bands (3571 and 632 cm^{-1}) and the PO_4^{3-} groups (especially at 962 cm^{-1}). This behaviour was associated with the incorporation of SiO_4^{4-} in the HAP structure [44].

FTIR spectrum of the sample AP-10MNa (Figure 6(d)) reveals the bands attributed to the vibration of PO_4^{3-} groups (553, 604, 946, 973, 1045 and 1124 cm^{-1}) characteristic of the β-TCP structure. Additionally, a new band is observed at 890 cm^{-1} attributed to vibrations of SiO_4^{4-} groups [26, 43].

Figure 7 shows the FTIR spectra of the AP-5MNa powder as a function of heat treatment at temperature from 200 °C to 1100 °C. The CO_3^{2-} bands disappeared between 700 °C and 900 °C and the OH^- bands intensities increased and became more intense at 900 °C. In addition, a new band appears at 890 cm^{-1} attributable to the SiO_4^{4-} group [25, 43]. At 1000 °C, we can see the OH^- bands loss indicating the decomposition of the HAP structure, in accordance with XRD results.

3.3. Specific surface area and size distribution

The specific surface area (SSA) results of as-dried powders are given in Table 3. It resulted that SSA value of the reference sample AP-0MNa prepared without MNa is close to 80 m^2/g. Addition of 2 wt% of MNa induces an increase in SSA value which attained 100.15 m^2/g. Further addition of MNa decreases in the SSA values of the nano-composites which attained 90.47 and 52.99 for AP-5MNa and AP-10MNa, respectively. The decrease in SSA value may be due to a decrease in the size of the crystals formed and/or to a change in the microstructure of the nano-biocomposite.

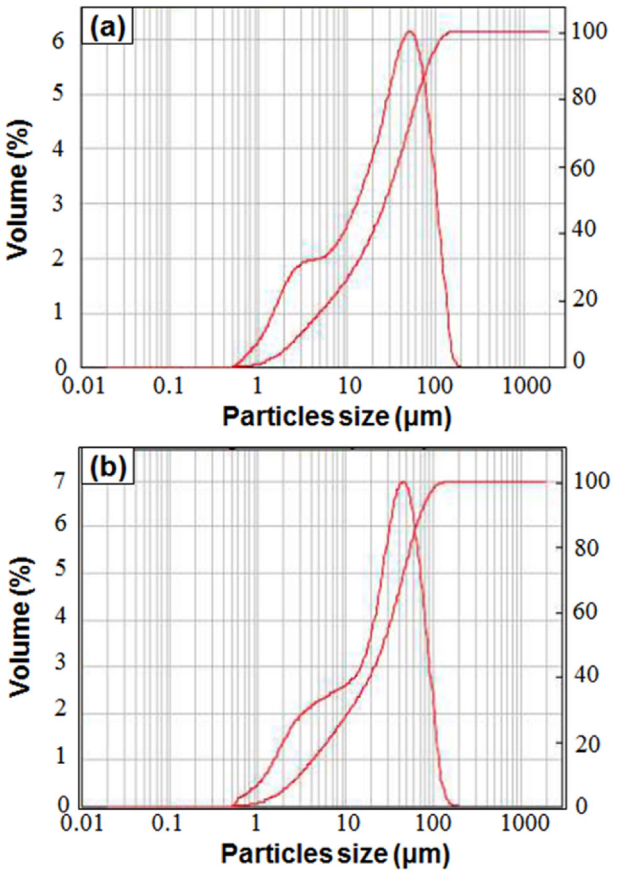

Figure 8. Size distribution of particle of as-dried samples: a) AP-0MNa and b) AP-10MNa and calcined at 900 °C: c) AP-0MNa and d) AP-10MNa.

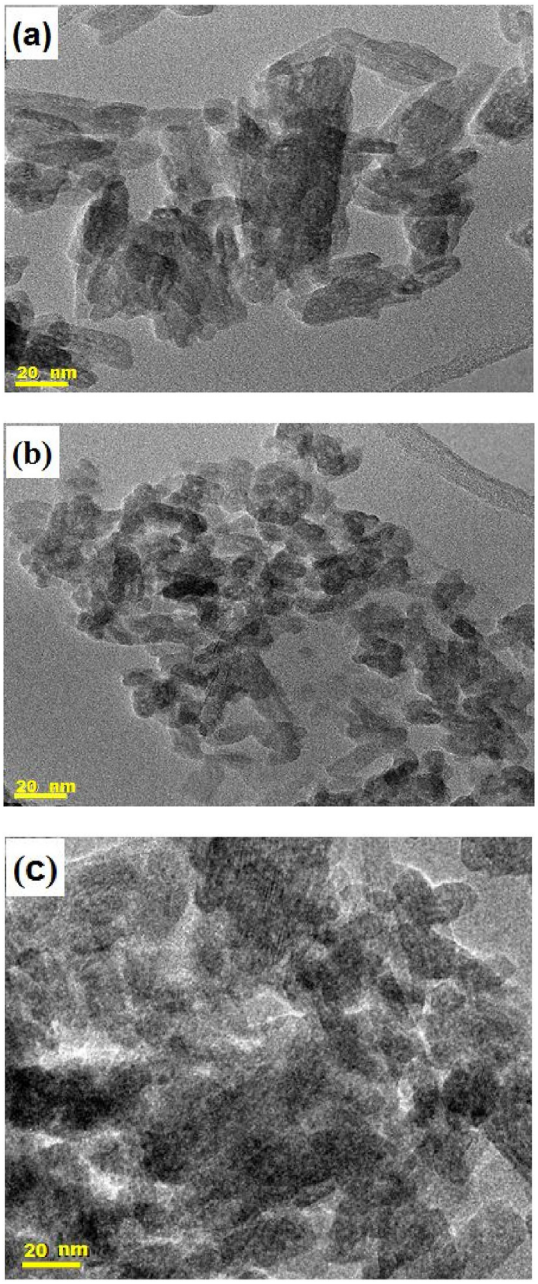

Figure 9. TEM images of as-dried particles: a) AP-0MNa, b) AP-2MNa and c) AP-10MNa.

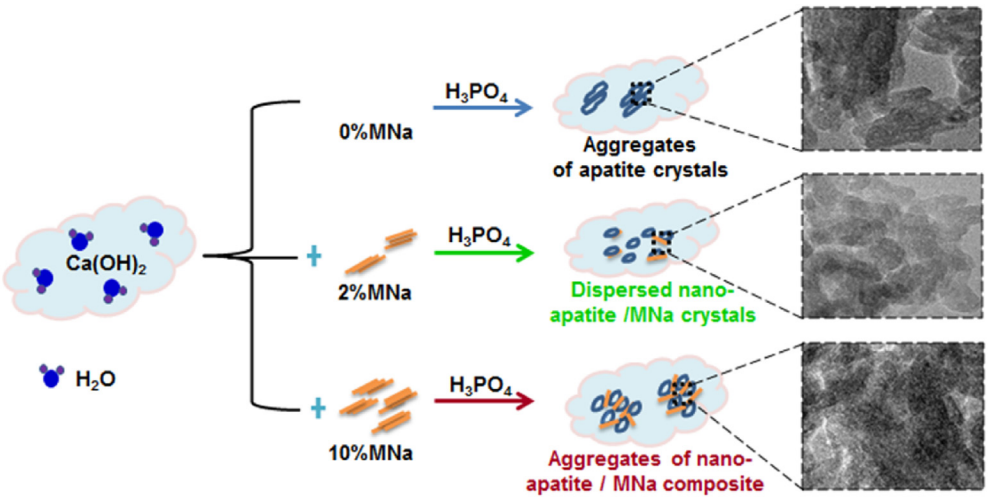

Figure 10. Schematic illustration of the microstructure of powders prepared with and without MNa.

Analyses of the particle size distribution were carried out on the dried and calcined powders (Figure 8). Two granulometric classes (0.166–7.9 μm and 7.9–291.6 μm) were identified for dried powders prepared without and with MNa (AP-0MNa and AP-10MNa). However, we can notice that the first population is slightly wider in the case of biocomposite.

After calcination of AP-0MNa and AP-10MNa samples at 900 °C, two granulometric classes (0.166–7.9 μm, 7.9–291.6 μm) were identified and also a new population at 250–1666 μm was identified as majority population for the sample AP-0MNa. For AP-10MNa, the particle size distribution has two populations: 1–125 μm and 125–1250 μm as majority population. These results indicate that the fine particles agglomerate in the presence of a significant amount of clay. Clay mineral therefore promotes the formation of compact microstructures when it's added in large quantity.

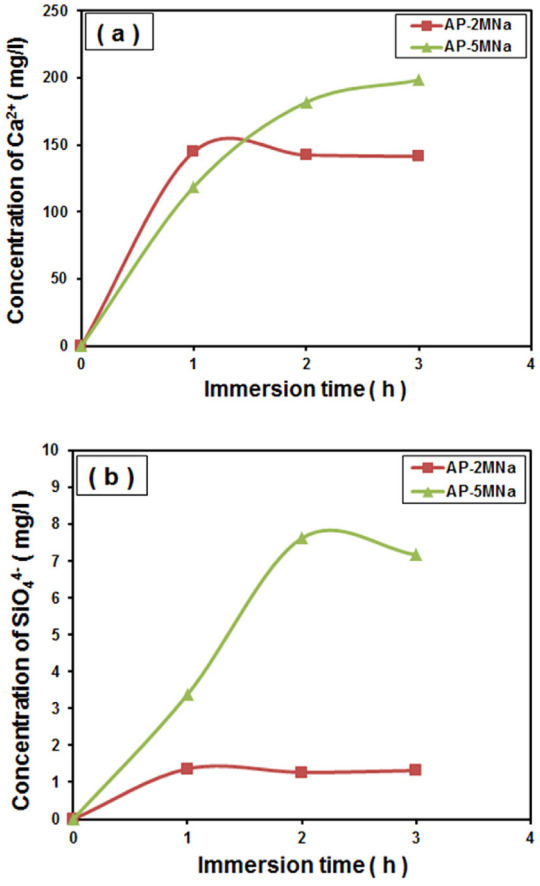

Figure 11. Dissolution rate of AP-2MNa and AP-5MNa composites: a) Ca^{2+} and b) SiO_4^{4-}.

3.4. Transmission electron microscopy (TEM)

The TEM analysis has been investigated on the powders after drying at 105 °C. The micrograph (Figure 9(a)) of AP-0MNa powder shows nano-particles with an average value of 33.41 nm in length and 4.23 nm in width. In the case of apatite synthesized with 2 wt% of MNa, the result (Figure 9(b)) shows that the size of the crystals becomes smaller with a decrease in the length which takes an average value of 22.66 nm. However, in the case of apatite synthesized with 10 wt% of MNa, the result (Figure 9(c)) shows small particles forming the agglomerates.

These results are consistent with specific surface area value. The incorporation of clay ions in to apatitic lattice leads to a decrease in the size particle and an increase in the specific surface. These results are in agreement with the literature which reports that the Si and Mg ions inhibit the grain growth of hydroxyapatite [44, 45].

Based on the results obtained in this study, we have graphically represented in Figure 10 the microstructure of the prepared powder composed of apatite tricalcium phosphate and of the apatite/MNa biocomposites. The graph shows that the addition of MNa reduces the size of the apatitic nanoparticles. A small amount of MNa improves their dispersion while higher amounts promote their agglomeration.

3.5. Dissolution behaviour

The biological properties of a composite material depend on its structure, microstructure and constituent materials. Biodegradation of biocomposites might be simulated by their dissolution in acidic solution. Therefore, establishing a dissolution comparison of calcium phosphates in acid medium appears to be of the paramount importance for the sintered biocomposites prepared in this study.

The results of dissolution tests are presented in Figures 11 and 12. The results show that the dissolution properties of the composites were affected by MNa. For both samples AP-2MNa and AP-5MNa with HAP structure, the concentration of Ca^{2+} and SiO_4^{4-} increased rapidly during the first hour of immersion. After 1h, the concentration of Ca^{2+} and SiO_4^{4-} remained unchanged over time for AP-2MNa, but for AP-5MNa the dissolution rate continues to increase. The sample AP-5MNa shows significantly higher Ca^{2+} and SiO_4^{4-} dissolution than AP-2MNa sample.

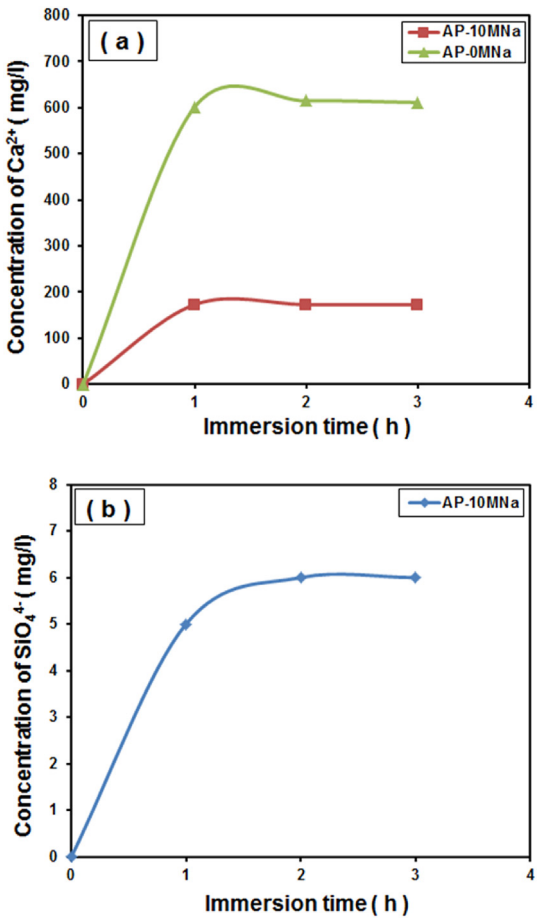

Figure 12. Dissolution rate of AP-0MNa and AP-10MNa composites: a) Ca^{2+} and b) SiO_4^{4-}.

This result is in agreement with the literature which reports that the dissolution rate of HAP was improved with incorporation of ions as SiO_4^{4-} [46], Mg^{2+} [47] and Na^{+} [48].

For both samples AP-0MNa and AP-10MNa with β-TCP structure, the concentration of Ca^{2+} also increased rapidly during the first hour. After 1h, the concentration of Ca^{2+} remained unchanged over time for both samples. The composite AP-10MNa shows significantly lower dissolution than the reference sample AP-0MNa prepared without MNa. The SiO_4^{4-} dissolution of AP-10MNa was faster during first hour. After 1h, the concentration of SiO_4^{4-} decreased and then remained constant. Hesaraki et al have reported the dissolution behavior of porous bodies (HAP/β-TCP) with and without MNa in Ringer's solution [23]. It was found that the addition of MNa decreased the dissolution rate of the porous bodies. A decrease in dissolution may be due to the presence of agglomerates.

On the other hand, it was reported that the dissolution rate of β-TCP decreased with incorporation of ions as Mg^{2+} [49, 50]. In our work, the simultaneous cationic and anionic incorporation of clay ions (e.g. SiO_4^{4-}, Al^{3+}, Mg^{2+} and Na^{+}) caused a significantly changes in the calcium phosphate structure of composites ceramics, which can explained the effect of MNa content on their dissolution behaviour.

The results show that *in-situ* precipitation of apatite/montmorillonite allowed us to develop a new class of biphasic and multiphasic phosphocalcic silicate composites.

The richness in trace elements makes clay a formidable mineralizer and the main advantage of the prepared biocomposites is their ability to release: Ca^{2+}, PO_4^{3-} and clay ions like SiO_4^{4-}, Na^{+} and Mg^{2+}, which stimulate bone growth and ensure good biological compatibility. So the contribution in the form of separate phases of the elements necessary for the formation of bone can constitute a new way to improve the bioactivity of phosphocalcic biomaterials.

4. Conclusion

In this study, apatitic calcium phosphate/MNa nano-composites were *in-situ* synthesized by reaction between calcium hydroxide and orthophosphoric acid (Ca/P atomic ratio = 1.50) in the presence of montmorillonite. The effect of amount of MNa on composition, structure and dissolution of the prepared composites was investigated. The results show that the MNa affected the composition and the type of the formed calcium phosphate phases by incorporation of clay ions into the apatitic structure. The content of MNa less than 10 wt% leads to the formation of HAP structure which decomposes at 1000 °C leading to the formation of β and α-TCP as secondary phases. However, the content of 10 wt% MNa stabilizes the β-TCP structure. The changes in the composition and crystal structure affect the dissolution properties of the prepared composites by increasing dissolution rate of HAP and a decreasing dissolution rate of β-TCP. The composition and improved dissolution of the multiphasic phosphocalcic silicate composite developed make it a potential synthetic bone substitute.

Declarations

Author contribution statement

M. Jamil: Performed the experiments; Analyzed and interpreted the data; Wrote the paper.

A. Elouahli: Performed the experiments; Analyzed and interpreted the data.

F. Abida, J. Assaoui, E. Gourri: Contributed reagents, materials, analysis tools or data.

Z. Hatim: Conceived and designed the experiments; Wrote the paper.

Funding statement

This research did not receive any specific grant from funding agencies in the public, commercial, or not-for-profit sectors.

Data availability statement

No data was used for the research described in the article.

Declaration of interests statement

The authors declare no conflict of interest.

Additional information

No additional information is available for this paper.

Acknowledgements

The authors express their sincere gratitude to Prof. Driss Zakria for X-ray Diffractometry analyzes at the Faculty of Sciences, Chouaib Doukkali University, El Jadida, Morocco.

References

[1] M. Ebrahimi, M.G. Botelho, S.V. Dorozhkin, Biphasic calcium phosphates bioceramics (HA/TCP): concept, physicochemical properties and the impact of standardization of study protocols in biomaterials research, Mater. Sci. Eng., C 71 (2017) 1293–1312.

[2] J.M. Bouler, P. Pilet, O. Gauthier, E. Verron, Biphasic calcium phosphate ceramics for bone reconstruction: a review of biological response, Acta Biomater. 53 (2017) 1–12.

[3] J.E. Maté-Sánchez de Val, P. Mazón, J.L. Calvo-Guirado, R.A.D. Ruiz, M.P. Ramírez Fernández, B. Negri, M. Abboud, P.N. De Aza, Comparison of three hydroxyapatite/β-tricalcium phosphate/collagen ceramic scaffolds: an in vivo study, J. Biomed. Mater. Res. 102 (2014) 1037–1046.

[4] T. Tanaka, H. Komaki, M. Chazono, S. Kitasato, A. Kakuta, S. Akiyama, K. Marumo, Basic research and clinical application of beta-tricalcium phosphate (β-TCP), Morphologie 101 (2017) 164–172.

[5] B.X. Vuong, Synthesis and characterization of HA/β-TCP bioceramic powder, Vietnam J. Chem. 56 (2018) 152–155.

[6] K. Kaviyarasu, A. Mariappan, K. Neyvasagam, A. Ayeshamariam, P. Pandi, R.R. Palanichamy, C. Gopinathan, G.T. Mola, M. Maaza, Photocatalytic performance and antimicrobial activities of HAp-TiO2 nanocomposite thin films by sol-gel method, Surface. Interfac. 6 (2017) 247–255.

[7] S.A. Ibraheem, E.A. Audu, M u Jaafar, J.A. Adudu, J.T. Barminas, V. Ochigbo, A. Igunnu, S.O. Malomo, Pectin from Parkia biglobosa pulp mediated green route synthesis of hydroxyapatite nanoparticles, Surface. Interfac. 17 (2019), 100360.

[8] S. Quillard, M. Paris, P. Deniard, R. Gildenhaar, G. Berger, L. Obadia, J.M. Bouler, Structural and spectroscopic characterization of a series of potassium- and/or sodium-substituted β-tricalcium phosphate, Acta Biomater. 7 (2011) 1844–1852.

[9] H. Khallok, A. Elouahli, S. Ojala, R.L. Keiski, A. Kheribech, Z. Hatim, Preparation of biphasic hydroxyapatite/β-tricalcium phosphate foam using the replication technique, Ceram. Int. 46 (14) (2020) 22581–22591.

[10] K. Salma-Ancane, L. Stipniece, A. Putnins, L. Berzina-Cimdina, Development of Mg-containing porous β-tricalcium phosphate scaffolds for bone repair, Ceram. Int. 41 (2015) 4996–5004.

[11] A. Rajabnejadkeleshteri, A. Kamyar, M. Khakbiz, Z.L. bakalani, H. Basiri, Synthesis and characterization of strontium fluor-hydroxyapatite nanoparticles for dental applications, Microchem. J. 153 (2020), 104485.

[12] K. Prem Ananth, S. Shanmugam, S.P. Jose, A.J. Nathanael, T.H. Oh, D. Mangalaraj, A.M. Ballamurugan, Structural and chemical analysis of silica-doped β-TCP ceramic coatings on surgical grade 316L SS for possible biomedical application, J. Asian Ceram. Soc. 3 (2015) 317–324.

[13] M.A. Goldberg, V.V. Smirnov, P.V. Protsenko, O.S. Antonova, S.V. Smirnov, A.A. Fomina, A.A. Konovalov, A.V. Leonov, A.A. Ashmarin, S.M. Barinov, Influence of aluminum substitutions on phase composition and morphology of β - tricalcium phosphate nanopowders, Ceram. Int. 43 (2017) 13881–13884.

[14] J.C. Elliott, Hydroxyapatite and nonstoichiometric apatites, in: Structure and chemistry of the apatites and other calcium orthophosphates vol. 18, 1994, pp. 111–189.

[15] E. Boanini, M. Gazzano, A. Bigi, Ionic substitutions in calcium phosphates synthesized at low temperature, Acta Biomater. 6 (2010) 1882–1894.

[16] M. Šupová, Substituted hydroxyapatites for biomedical applications: a review, Ceram. Int. 41 (2015) 9203–9231.

[17] B. Yilmaz, A.Z. Alshemary, Z. Evis, Co-doped hydroxyapatites as potential materials for biomedical applications, Microchem. J. 144 (2019) 443–453.

[18] M. Mousa, N.D. Evans, R.O.C. Oreffo, J.I. Dawson, Clay nanoparticles for regenerative medicine and biomaterial design: a review of clay bioactivity, Biomaterials 159 (2018) 204–214.

[19] A. Olad, F. Farshi Azhar, The synergetic effect of bioactive ceramic and nanoclay on the properties of chitosan–gelatin/nanohydroxyapatite–montmorillonite scaffold for bone tissue engineering, Ceram. Int. 40 (2014) 10061–10072.

[20] C. Viseras, P. Cerezo, R. Sanchez, I. Salcedo, C. Aguzzi, Current challenges in clay minerals for drug delivery, Appl. Clay Sci. 48 (2010) 291–295.

[21] A. Borrego-Sánchez, E. Carazo, C. Aguzzi, C. Viseras, C.I. Sainz-Díaz, Biopharmaceutical improvement of praziquantel by interaction with montmorillonite and sepiolite, Appl. Clay Sci. 160 (2018) 173–179.

[22] Q. Yuan, T.D. Golden, A novel method for synthesis of clay/polymer stabilized silver nanoparticles, Surface. Interfac. 20 (2020), 100620.

[23] S. Hesaraki, A. Zamani, M. Hafezi, Montmorillonite-added calcium phosphate bioceramic foams, Key Eng. Mater. 361–363 (2008) 111–114.

[24] R. Nawang, M.Z. Hussein, K.A. Matori, C.A. Che Abdullah, M. Hashim, Physicochemical properties of hydroxyapatite/montmorillonite nanocomposite prepared by powder sintering, Results Phys. 15 (2019), 102540.

[25] M. Jamil, A. Elouahli, F. Abida, H. Khallok, E. Gourri, A. Kheribech, Z. Hatim, Development of triphasic hydroxyapatite/(α and β)-tricalcium phosphate based composites by sintering powder of calcium-apatite in the presence of montmorillonite, J. Inorg. Organomet. Polym. Mater. 30 (2020) 2489–2498.

[26] M. Jamil, A. Elouahli, H. Khallok, B. El ouatli, Z. Hatim, Characterization of β-tricalcium phosphate-clay mineral composite obtained by sintering powder of apatitic calcium phosphate and montmorillonite, Surface. Interfac. 17 (2019), 100380.

[27] K.S. Katti, D.R. Katti, R. Dash, Synthesis and characterization of a novel chitosan/montmorillonite/hydroxyapatite nanocomposite for bone tissue engineering, Biomed. Mater. 3 (2008), 034122.

[28] A. Ambre, K.S. Katti, D.R. Katti, In situ mineralized hydroxyapatite on amino acid modified nanoclays as novel bone biomaterials, Mater. Sci. Eng., C 31 (2011) 1017–1029.

[29] L. Pazourková, K.Č. Barabaszová, M. Hundáková, Proceedings of 5th International Conference NANOCON, 2013, pp. 83–88.

[30] H. Khallok, S. Ojala, M. Ezzahmouly, A. Elouahli, E.H. Gourri, M. Jamil, Z. Hatim, Porous foams based hydroxyapatite prepared by direct foaming method using egg white as a pore promoter, J. Australas. Ceram. Soc. 55 (2019) 611–619.

[31] Z. Wen You, A.B.M. Rabie, R.W.K. Wong, T. Bin, 3rd International Nanoelectronics Conference (INEC), 2010, 2010, pp. 817–818.

[32] A. Elouahli, H. Khallok, Z. Hatim, Neutralization method for tricalcium phosphate production: optimization using response surface methodology, Surface. Interfac. 15 (2019) 100–109.

[33] P. Scherrer, Bestimmung der inneren Struktur und der Größe von Kolloidteilchen mittels Röntgenstrahlen, Kolloidchemie Ein Lehrbuch, Springer, 1912, pp. 387–409.

[34] M.J. Glimcher, L.C. Bonar, M.D. Grynpas, W.J. Landis, A.H. Roufosse, Recent studies of bone mineral: is the amorphous calcium phosphate theory valid? J. Cryst. Growth 53 (1981) 100–119.

[35] R. Riihonen, C.T. Supuran, S. Parkkila, S. Pastorekova, H.K. Väänänen, T. Laitala-Leinonen, Membrane-bound carbonic anhydrases in osteoclasts, Bone 40 (2007) 1021–1031.

[36] L. Brisson, S.J. Reshkin, J. Goré, S. Roger, pH regulators in invadosomal functioning: proton delivery for matrix tasting, Eur. J. Cell Biol. 91 (2012) 847–860.

[37] M.L. Rozalén, F.J. Huertas, P.V. Brady, J. Cama, S. García-Palma, J. Linares, Experimental study of the effect of pH on the kinetics of montmorillonite dissolution at 25°C, Geochem. Cosmochim. Acta 72 (2008) 4224–4253.

[38] M. Rozalen, F.J. Huertas, P.V. Brady, Experimental study of the effect of pH and temperature on the kinetics of montmorillonite dissolution, Geochem. Cosmochim. Acta 73 (2009) 3752–3766.

[39] R.G. Carrodeguas, A.H. De Aza, X. Turrillas, P. Pena, S. De Aza, New approach to the β→α polymorphic transformation in magnesium-substituted tricalcium phosphate and its practical implications, J. Am. Ceram. Soc. 91 (2008) 1281–1286.

[40] I. Cacciotti, A. Bianco, High thermally stable Mg-substituted tricalcium phosphate via precipitation, Ceram. Int. 37 (2011) 127–137.

[41] S.V. Dorozhkin, Biphasic, triphasic and multiphasic calcium orthophosphates, Acta Biomater. 8 (2012) 963–977.

[42] F. Abida, M. Elassfouri, M. Ilou, M. Jamil, N. Moncif, Z. Hatim, Tricalcium phosphate powder: preparation, characterization and compaction abilities, Mediterr. J. Chem. 6 (2017) 71–76.

[43] C.-W. Song, T.-W. Kim, D.-H. Kim, H.-H. Jin, K.-H. Hwang, J.K. Lee, H.-C. Park, S.-Y. Yoon, In situ synthesis of silicon-substituted biphasic calcium phosphate and their performance in vitro, J. Phys. Chem. Solid. 73 (2012) 39–45.

[44] L.T. Bang, K. Ishikawa, R. Othman, Effect of silicon and heat-treatment temperature on the morphology and mechanical properties of silicon - substituted hydroxyapatite, Ceram. Int. 37 (2011) 3637–3642.

[45] B. Gayathri, N. Muthukumarasamy, D. Velauthapillai, S.B. Santhosh, V. asokan, Magnesium incorporated hydroxyapatite nanoparticles: preparation, characterization, antibacterial and larvicidal activity, Arab. J. Chem. 11 (2018) 645–654.

[46] H. Yu, K. Liu, F. Zhang, W. Wei, C. Chen, Q. Huang, Microstructure and in vitro bioactivity of silicon-substituted hydroxyapatite, Silicon 9 (2017) 543–553.

[47] X. Lijuan, J. Liuyun, X. Chengdong, J. Lixin, Effect of different synthesis conditions on the microstructure, crystallinity and solubility of Mg-substituted hydroxyapatite nanopowder, Adv. Powder Technol. 25 (2014) 1142–1146.

[48] J. Sang Cho, S.-H. Um, D. Su Yoo, Y.-C. Chung, S. Hye Chung, J.-C. Lee, S.-H. Rhee, Enhanced osteoconductivity of sodium-substituted hydroxyapatite by system instability, J. Biomed. Mater. Res. B Appl. Biomater. 102 (2014) 1046–1062.

[49] J. Walker, S. Shadanbaz, T.B.F. Woodfield, M.P. Staiger, G.J. Dias, Magnesium biomaterials for orthopedic application: a review from a biological perspective, J. Biomed. Mater. Res. B Appl. Biomater. 102 (2014) 1316–1331.

[50] G. Tripathi, Y. Sugiura, K. Tsuru, K. Ishikawa, In vivo stability evaluation of Mg substituted low crystallinity ß-tricalcium phosphate granules fabricated through dissolution–precipitation reaction for bone regeneration, Biomed. Mater. 13 (2018), 65002.